Twisted photon entanglement through turbulent air across Vienna

Mario Krenn[a,b,1], Johannes Handsteiner[a,b], Matthias Fink[a,b], Robert Fickler[a,b,2], and Anton Zeilinger[a,b,1]

[a]Vienna Center for Quantum Science and Technology, Faculty of Physics, University of Vienna, A-1090 Vienna, Austria; and [b]Institute for Quantum Optics and Quantum Information, Austrian Academy of Sciences, A-1090 Vienna, Austria

Photons with a twisted phase front can carry a discrete, in principle, unbounded amount of orbital angular momentum (OAM). The large state space allows for complex types of entanglement, interesting both for quantum communication and for fundamental tests of quantum theory. However, the distribution of such entangled states over large distances was thought to be infeasible due to influence of atmospheric turbulence, indicating a serious limitation on their usefulness. Here we show that it is possible to distribute quantum entanglement encoded in OAM over a turbulent intracity link of 3 km. We confirm quantum entanglement of the first two higher-order levels (with OAM$=\pm 1\hbar$ and $\pm 2\hbar$). They correspond to four additional quantum channels orthogonal to all that have been used in long-distance quantum experiments so far. Therefore, a promising application would be quantum communication with a large alphabet. We also demonstrate that our link allows access to up to 11 quantum channels of OAM. The restrictive factors toward higher numbers are technical limitations that can be circumvented with readily available technologies.

quantum entanglement | photonic orbital angular momentum | quantum communication | large Hilbert space | photonic spatial modes

Long-distance quantum entanglement with photons opens up the possibility to test fundamental properties of quantum physics in regimes not accessible in laboratory-scale experiments, it can be used for quantum communication between widely separated parties, and it is the basis of quantum repeaters as nodes in a global quantum network. As the polarization of photons is easily controllable and resistant against atmospheric turbulences, it has been successfully used in a variety of different long-distance quantum experiments (1–4). However, polarization of photons resides in a two-dimensional state space, restricting the complexity of entangled states both for certain quantum communication tasks and for fundamental tests.

In contrast with polarization, the orbital angular momentum (OAM) modes of photons have an unbounded state space. Photons carrying OAM have a twisted wave front with a phase that varies from 0 to $2\pi\ell$ in the azimuthal direction. Here, ℓ is an integer which stands for the topological charge, and $\ell \cdot \hbar$ is the OAM of the photon. Such states can carry larger amount of information per photon. It also allows more complex types of nonclassical correlations, such as entanglement of large quantum numbers (5) or high-dimensional entanglement (6–10). However, the possibility of more complex entangled quantum states poses a substantial challenge due to the negative influence of atmospheric turbulences on such modes. Several theoretical (11–17) and laboratory-scale (18–20) studies investigated the effect of turbulence on entanglement encoded in the OAM of photons, and many others explore the influence of turbulence on OAM modes in general (21–24). Only one quantum experiment was carried out beyond the laboratory scale, by performing a quantum communication protocol over 210 m using a polarization–OAM hybrid system (25). It was located in a large hall to minimize the disturbing effects of turbulence. So far, no experiment at the quantum level has been performed in a long-distance turbulent real-world environment, and quantum entanglement has not yet been demonstrated beyond the laboratory scale with photons carrying OAM.

Results

Recently, in two experiments the classical transmission of OAM modes in a long-distance outdoor environment has been investigated. The first experiment was performed over a 3-km intracity link in Vienna (the same link that is being used in the experiment presented here). Superpositions of OAM modes have been used, which can be categorized by their intensity structure. A pattern recognition algorithm distinguished the different modes with high quality. The results also indicated that the phase of OAM superpositions is well conserved during the transmission, hinting that the distribution of quantum entanglement encoded in OAM might be possible (26). Shortly after that, a second experiment was performed over a 1.6-km intracity link in Erlangen (27). There, an OAM mode sorter (28) has been used to categorize different states from $\ell = -2$ to $\ell = +2$. A significant broadening of the OAM spectra has been observed. Here, we present the results of an experiment in which we confirm the indication of the first experiment mentioned above: We show that quantum entanglement distribution with spatial modes is possible over a turbulent intracity link.

The experimental setup can be divided into four main parts (Fig. 1): the source of polarization entanglement, the transfer of one photon from polarization to the OAM degree of freedom, Alice's polarization analysis, and Bob's OAM measurement after transmission. The sender (Alice) and the receiver (Bob) are at different physical locations 3 km apart. The sender

Significance

The spatial structure of photons provides access to a very large state space. It enables the encoding of more information per photon, useful for (quantum) communication with large alphabets and fundamental studies of high-dimensional entanglement. However, the question of the distribution of such photons has not been settled yet, as they are significantly influenced by atmospheric turbulence in free-space transmissions. In the present paper we show that it is possible to distribute quantum entanglement of spatially structured photons over a free-space intracity link. We demonstrate the access to four orthogonal quantum channels in which entanglement can be distributed over large distances. Furthermore, already available technology could provide access to even larger quantum state spaces.

PHYSICS

Fig. 1. Sketch of the experimental setup. The experiment takes place at two locations separated by 3 km. The sender is located in a radar tower of ZAMG; the receiver is the Hedy Lamarr Quantum Communication Telescope at the rooftop of our institute IQOQI. (*Left*) At the sender, we have a high-fidelity Sagnac-type polarization entanglement source. Whereas photon A remains in the polarization degree of freedom, photon B is transferred to OAM, using an interferometric scheme (5, 29): In it, the photon's path is separated according to its polarization at a polarizing beam splitter (PBS) and transformed to an OAM value depending on its path using a spatial light modulator (SLM, Hamamatsu LCOS-SLM). After recombination of the paths, the transfer is completed by deleting the polarization information with a polarizer (Pol). Subsequently, the photon wave front is expanded and sent to the transceiver with a high-quality lens. Meanwhile photon A of the entangled pair is delayed in a 30-m fiber to ensure the transfer and sending of photon B before photon A is detected. After the fiber photon A is measured using a half-wave plate (λ/2) or a quarter-wave plate (λ/4)—depending on the basis in question—a PBS and two APDs. The detection times of the photons are recorded with a TTM. (*Right*) At the receiver, the transmitted photons are collected by a Newton-type telescope with a primary mirror of 37-cm diameter. In front of the primary mirror, opaque masks with symmetric slit patterns are used to perform mode measurements (Fig. 2). An iris (I) and a 3-nm band-pass filter (IF) were used to minimize background light. The photons are detected with an APD, and time tagged with a TTM. Coincidences are then extracted by comparing the time-tagging information from both locations.

is located in an ∼35-m-high radar tower of *Zentralanstalt für Metrologie und Geodynamik* (ZAMG: Central Institute for Metrology and Geodynamics). There we use a high-fidelity, high-brightness polarization entanglement source (30, 31) with an uncorrected average visibility of ∼97.5%. Photon A is unchanged, whereas photon B's polarization state is transferred interferometrically to an OAM state (5). After the transfer the generated hybrid-entangled quantum state can be written as

$$|\psi\rangle = \frac{1}{\sqrt{2}}(|H\rangle_A|+\ell\rangle_B + |V\rangle_A|-\ell\rangle_B). \qquad [1]$$

To ensure that photon B is transferred and sent before photon A is measured, we delay photon A by a 30-m fiber. It ensures that the detection of the two entangled photons is space-like separated: Any signal from one measurement to the other would need to propagate faster than the speed of light to influence the result. Afterward the polarization of photon A is measured with a two-output polarization analyzing station. Each detection event is time-stamped and recorded with a time-tagging module (TTM; Austrian Institute of Technology TTM 8000). The OAM-encoded photon B is magnified to a Gaussian beam waist of 11 mm and sent through turbulent atmosphere with a high-quality lens (best-form f/4 doublet lens, with low spherical aberrations) using a focal length of f = 30 cm to the receiver 3 km away.

At the receiver on the rooftop of our institute [Institute for Quantum Optics and Quantum Information (IQOQI) Vienna],

we use a Newton-type telescope with a primary mirror of 37-cm diameter and a focal length of f = 1.2m. In front of the primary mirror, we use an absorptive mask with a transparent, symmetric slit pattern to measure the modes (Fig. 2). The technique (5) allows us to measure visibilities in OAM-superposition bases, which is sufficient to verify entanglement. The masks are 40 cm in diameter and have a slit opening angle of 16° and 5.6° (for ℓ = 1 and ℓ = 2, respectively). The transmitted light is then detected on an avalanche photon detector (APD) with an active area of 500-μm diameter. Similarly to the detection of the polarized partner photons, the arrival times are time tagged with a second TTM. To synchronize the time stamps on the two remote locations in the subnanosecond regime, we directly use the time correlation of the photon pairs (which is inherently below 1 ps), as explained in ref. 32.

In the experiment, we perform visibility measurements in two mutually unbiased bases (MUBs). For photon A, the bases are diagonal or antidiagonal and right- or left-circular polarization ($|\psi_x\rangle = |H\rangle \pm |V\rangle$ and $|\psi_y\rangle = |H\rangle \pm i|V\rangle$). For photon B, we measure in the superposition bases of two opposite OAMs, specifically ($|\psi_x\rangle = |+\ell\rangle \pm |-\ell\rangle$ and $|\psi_y\rangle = |+\ell\rangle \pm i|-\ell\rangle$). Here, the superposition structure is a ring with 2ℓ intensity maxima and minima. By changing the phase of the superposition, the intensity structure is rotated. With the slit mask, we can measure photons in the σ_x and σ_y bases, which correspond to the σ_x and σ_y bases of photon A (5). Specifically, we measure fringes in coincidence counts for changing angular positions of the mask.
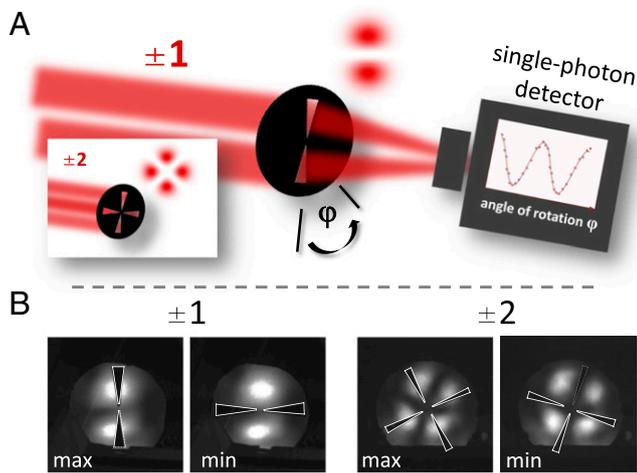
Fig. 2. Principle of the measurement technique. The superposition of two OAM modes with opposite ℓ has 2ℓ minima and maxima in a ring. The angular orientation depends on the relative phase. We use a mask, which resembles the symmetry of the beam, to measure correlations. (*A*) An incoming beam hits the mask. For $\ell = \pm 1$, an opaque mask with two transparent slits is used to measure different superposition states. A detector after the mask collects all photons passing the slits. The superposition of $\ell = \pm 2$ has four paddles, thus we use a mask with four slits. (*B*) Images of an alignment laser beam at the mask (mounted at the telescope at IQOQI, slits are highlighted) after 3-km transmission. The laser is in a superposition of $\ell = \pm 1$ and $\ell = \pm 2$. The angular position of the mask is set to the maximum and to the minimum. In the entanglement experiment, we see the fringes only in coincidences.

We find minima and maxima of coincidences (Fig. 3), and calculate the visibility:

$$\text{vis} = \frac{\max_1 - \min_1 + \max_2 - \min_2}{\max_1 + \min_1 + \max_2 + \min_2}.$$

"max" and "min" are highlighted with circles in Fig. 3. To verify entanglement, we use an entanglement witness, which is the sum of the two visibilities in the two MUBs (33):

$$W = \text{vis}_x + \text{vis}_y \begin{cases} \leq 1 : \text{separable} \\ > 1 : \text{entangled} \end{cases}. \qquad [2]$$

All separable quantum states can reach at most $W = 1$, which can be understood intuitively: If a product state is perfectly correlated in one basis, it cannot be correlated in any other MUBs. Any experimental value above $W = 1$ verifies entanglement in the system (a maximally entangled quantum state can have perfect visibility in both bases, thus $W = 2$). The visibilities are calculated directly from the maxima and minima of the measured coincidences (blue/red and yellow/green circles in Fig. 3).

In the first measurement, we use the first higher-order mode with $\ell = 1$. We accumulate coincidence detections over 20 s at 20 different angular positions of the mask with a resolution of 9° (Fig. 3). The coincidence window is 2.5 ns. Without any corrections (such as accidental coincidence subtraction) and without any assumption about the photon statistics, we get

$$W_{\ell=1} = 1.3644 \pm 0.0084,$$

which statistically significantly confirms entanglement between the two distant photons. The error stands for the SD of the mean. We calculate the error by dividing the 20-s interval at each measurement position into 20 sections of equal length, and calculate the

witness equation **2** for each of the 20 sections individually. From the resulting 20 values for $W_{\ell=1}$ (see the *Supporting Information*), we calculate the mean value and its uncertainty. To calculate the uncertainty of $W_{\ell=1}$, we did not need to assume any specific photon statistics. In many cases, Poissonian distribution is a good approximation of the photon statistics. However, it neglects additional sources of fluctuations, which can become relevant in experiments without controlled environments, such as free-space experiments. If we had assumed Poissonian distribution in our experiment, we would have underestimated the uncertainty significantly by around 70%, which is mainly due to atmospheric turbulences and instabilities at the sender. If we subtract accidental counts ($\sim 85 \pm 3$ counts per s), the average visibility in both bases will be roughly 84.2%. The visibility is enough to violate a Bell-type inequality, which would lead to violation of local realism and to the possibility of device-independent quantum key distribution.

In a second experiment, we transfer the photon to $\ell = 2$ before transmission, send it to the receiver, and measure coincidence counts for 20 different mask positions, each 4.5° rotated, for 40 seconds per setting. Here we get

$$W_{\ell=2} = 1.139 \pm 0.021,$$

verifying entanglement with $\ell = 2$. Again, the error stands for the SD of the mean, which has been evaluated equivalently as before: 40-second measurement intervals are divided into 40 parts of 1-second length. It results in 40 independent values of $W_{\ell=2}$ (see the *Supporting Information*), from which the mean and its error was obtained. Note that again we did not assume any information about the photon statistics. However, we had to subtract accidental coincidence counts ($\sim 95 \pm 7$/s, but measured for each measurement setting individually, see the *Supporting Information*), because the signal-to-noise ratio was significantly higher (5.5% for $\ell = 2$ compared with 36.0% for $\ell = 1$), which can be understood from the different weather conditions during that night, different detection efficiency at the telescope, and smaller slit size of the masks (more details in the *Supporting Information*). As we collect timing information of the photons at the sending and receiving stations, we can access the number of accidental counts directly: At the offset between the time-tagging clocks, which correspond to the arrival times of the photons from a pair at the two locations, real coincidence counts from the entangled pairs are found. At every other offset, accidental coincidences can be seen (see the *Supporting Information*).

In both experiments for $\ell = 1$ and $\ell = 2$, we find visibilities smaller than unity. The reasons are an imperfect entanglement source (due to lack of temperature and vibration stabilization), imperfect detection method (the mask method can only give unity visibility for infinitesimal small slits), imperfect polarization compensation in fibers, accidental coincidence counts, and atmospheric influence. The first-order atmospheric influences are tip and tilt of the beam, which leads to relative misalignment between the mode and the mask. As the detection method is axis-dependent, it results in a significant drop in visibility (see the *Supporting Information*), which is larger for higher-order modes. However, that effect could be compensated with readily available adaptive optics.

Having confirmed that entanglement encoded in OAM can be transmitted over an intracity link, we estimate the number of different orthogonal quantum channels we have access to in principle. As OAM modes grow for higher numbers of ℓ and our receiver telescope has a finite size, there is a maximum number of ℓ that can be detected. For that, we transfer photon B to different values of ℓ and (from $\ell = 0$–15) and record the number of coincidences with photon A. Thus, photon A is a trigger for the higher-order ℓ modes of photon B after sending it across the city. Here, no mask is in front of the telescope. The detected

$$|\psi\rangle = \frac{1}{\sqrt{2}}\left(|H\rangle_A|+1\rangle_B + |V\rangle_A|-1\rangle_B\right)$$

$$|\psi\rangle = \frac{1}{\sqrt{2}}\left(|H\rangle_A|+2\rangle_B + |V\rangle_A|-2\rangle_B\right)$$
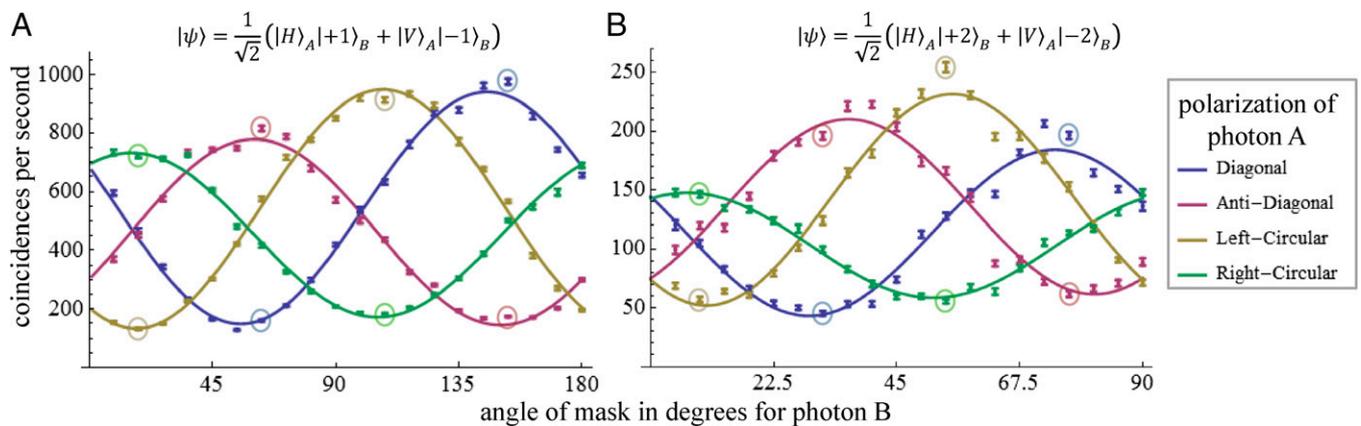
Fig. 3. Coincidences between the transmitted photon encoded in OAM and the locally measured polarization photon. For four different polarization settings at Alice's photon A, coincidences were recorded for 20 different angular positions of the mask at Bob's receiver. Error bars are the SD of the mean, calculated without assumptions about the underlying photon distribution from raw data by splitting the whole measurement time into 1-s intervals. The circles indicate the data used to calculate the entanglement witness. The two maxima (minima) per basis are denoted as max_1 and max_2 (min_1 and min_2) for calculating the visibility vis in the σ_x and σ_y bases. (A) Raw coincidences for $\ell = 1$. Coincidences for each angular position at the receiver are measured for 20 s. (B) For $\ell = 2$, we subtract accidental counts. Here, the coincidence counts for each angular position are measured for 40 s.

coincidence rates in Fig. 4 show that photons up to $\ell = 5$ can be distinguished from the background. The graph can be described very well by the geometry of our telescope, which cuts the incoming beam both at the primary and secondary mirror (*Supporting Information*). We consider the counts of high order ($\ell \geq 10$) as background, as they reach an asymptotic value (*Supporting Information*). With our sender and receiver, we have access to roughly 11 quantum channels of OAM ($\ell = 0$ to $\ell = \pm 5$).

Discussion

In conclusion, we are able to verify quantum entanglement of photon pairs with spatial modes over a turbulent, real-world link of 3 km across Vienna. It shows that the spatial phase structure of single photons is preserved sufficiently well to be used in quantum optical experiments involving entanglement. By using the first two higher-order structures ($\ell = \pm 1$, $\ell = \pm 2$), we show that at least four additional orthogonal channels [in addition to the zeroth-order Gaussian (1) case for $\ell = 0$] permit long-distance quantum communication. Although we still use two-dimensional subspaces, our result clearly shows that entanglement encoded in OAM can be identified after long-distance transmission. It is not fundamentally limited by atmospheric turbulences, as expected in some recent investigation, and thus could be a feasible way to distribute high-dimensional entanglement.

We also show that our quantum link allows up to 11 orthogonal channels of OAM. The restrictive factors toward a higher number of channels and higher quality of entanglement detection are technical limitations. The number of accessible channels can be increased by using optimal generations of the modes (leading to smaller intensity structures) (34, 35) and larger sending and receiving telescopes. The quality of disturbed spatial modes can be improved with well-established adaptive phase-correction algorithms (24, 36, 37), which might lead to significantly larger quality in the entanglement identification. Adaptive measurement algorithms form another method to improve the entanglement detection, by adjusting the measurements according to the turbulence (38).

Entanglement of high-order spatially encoded modes over long distance opens up several interesting directions: Firstly, twisted photons have a large state space, and thus can carry more information than the well-studied case of polarization. Higher information capacity could be interesting for both classical and quantum communication, for example to increase the data rate. Additionally, in quantum key distribution (39–41) it could be used

for increasing the robustness against noise, or improving the security against advanced eavesdroppers (42). Secondly, OAM of photons permits complex types of entanglement due to their large state space. It also represents a physical quantity which can be (in principle) arbitrarily large, thus it might be a very interesting testbed for fundamental tests. As such, curious phenomena such as the coupling of OAM modes with the space–time metric have been proposed (43). We believe that our results will motivate both further theoretical and experimental research into the promising novel direction of long-distance quantum experiments with twisted photons.
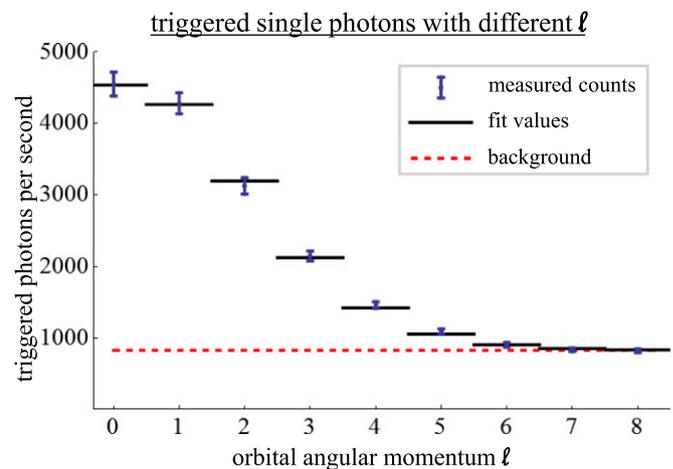
triggered single photons with different ℓ

Fig. 4. Triggered single-photon counts for different orbital angular momentum l. We use correlated photon pairs (blue, each point is measured for 60 s) to determine the number of accessible OAM modes at the telescope. For that, we measure one photon at the sender, and transfer the correlated partner photon to a higher-order OAM mode (from $\ell = 0$ to $\ell = 8$), which is then transmitted to the telescope 3 km away. The lower rate of coincidence counts for higher-order modes is due to the geometric restrictions (finite size of primary and secondary mirror) of the telescope, which can be modeled very well (black line; see the *Supporting Information*). The error bars show the SD. The red dashed line indicates the background counts (calculated from average counts of $\ell = 10$ to $\ell = 15$). The data show that we are able to access modes up to $\ell = 5$ from the background, which constitutes 11 orthogonal quantum channels ($\ell = -5$ to $\ell = 5$).

1. Ursin R, Tiefenbacher F, Schmitt-Manderbach T, Weier H, Scheidl T, Lindenthal M, Zeilinger A (2007) Entanglement-based quantum communication over 144 km. *Nat Phys* 3(7):481–486.
2. Yin J, et al. (2012) Quantum teleportation and entanglement distribution over 100-kilometre free-space channels. *Nature* 488(7410):185–188.
3. Ma XS, et al. (2012) Quantum teleportation over 143 kilometres using active feed-forward. *Nature* 489(7415):269–273.
4. Erven C, Meyer-Scott E, Fisher K, Lavoie J, Higgins BL, Yan Z, Resch KJ (2014) Experimental three-photon quantum nonlocality under strict locality conditions. *Nat Photon* 8(4):292–296.
5. Fickler R, et al. (2012) Quantum entanglement of high angular momenta. *Science* 338(6107):640–643.
6. Agnew M, Leach J, McLaren M, Roux FS, Boyd RW (2011) Tomography of the quantum state of photons entangled in high dimensions. *Phys Rev A* 84(6):062101.
7. Dada AC, Leach J, Buller GS, Padgett MJ, Andersson E (2011) Experimental high-dimensional two-photon entanglement and violations of generalized Bell inequalities. *Nat Phys* 7(9):677–680.
8. Romero J, Giovannini D, Franke-Arnold S, Barnett SM, Padgett MJ (2012) Increasing the dimension in high-dimensional two-photon orbital angular momentum entanglement. *Phys Rev A* 86(1):012334.
9. Giovannini D, et al. (2013) Characterization of high-dimensional entangled systems via mutually unbiased measurements. *Phys Rev Lett* 110(14):143601.
10. Krenn M, et al. (2014) Generation and confirmation of a (100 x 100)-dimensional entangled quantum system. *Proc Natl Acad Sci USA* 111(17):6243–6247.
11. Gopaul C, Andrews R (2007) The effect of atmospheric turbulence on entangled orbital angular momentum states. *New J Phys* 9(4):94.
12. Tyler GA, Boyd RW (2009) Influence of atmospheric turbulence on the propagation of quantum states of light carrying orbital angular momentum. *Opt Lett* 34(2):142–144.
13. Sheng X, Zhang Y, Zhao F, Zhang L, Zhu Y (2012) Effects of low-order atmosphere-turbulence aberrations on the entangled orbital angular momentum states. *Opt Lett* 37(13):2607–2609.
14. Brünner T, Roux FS (2013) Robust entangled qutrit states in atmospheric turbulence. *New J Phys* 15(6):063005.
15. Alonso JRG, Brun TA (2013) Protecting orbital-angular-momentum photons from decoherence in a turbulent atmosphere. *Phys Rev A* 88(2):022326.
16. Roux FS, Konrad T (2014) Parameter dependence in the atmospheric decoherence of modally entangled photon pairs. *Phys Rev A* 90(5):052115.
17. Leonhard ND, Shatokhin VN, Buchleitner A (2015) Universal entanglement decay of photonic-orbital-angular-momentum qubit states in atmospheric turbulence. *Phys Rev A* 91(1):012345.
18. Pors BJ, Monken CH, Eliel ER, Woerdman JP (2011) Transport of orbital-angular-momentum entanglement through a turbulent atmosphere. *Opt Express* 19(7):6671–6683.
19. Ibrahim AH, Roux FS, McLaren M, Konrad T, Forbes A (2013) Orbital-angular-momentum entanglement in turbulence. *Phys Rev A* 88(1):012312.
20. da Cunha Pereira MV, Filpi LA, Monken CH (2013) Cancellation of atmospheric turbulence effects in entangled two-photon beams. *Phys Rev A* 88(5):053836.
21. Paterson C (2005) Atmospheric turbulence and orbital angular momentum of single photons for optical communication. *Phys Rev Lett* 94(15):153901.
22. Lukin VP, Konyaev PA, Sennikov VA (2012) Beam spreading of vortex beams propagating in turbulent atmosphere. *Appl Opt* 51(10):C84–C87.
23. Ren Y, et al. (2013) Atmospheric turbulence effects on the performance of a free space optical link employing orbital angular momentum multiplexing. *Opt Lett* 38(20):4062–4065.
24. Rodenburg B, Mirhosseini M, Malik M, Magaña-Loaiza OS, Yanakas M, Maher L, Boyd RW (2014) Simulating thick atmospheric turbulence in the lab with application to orbital angular momentum communication. *New J Phys* 16(3):033020.
25. Vallone G, et al. (2014) Free-space quantum key distribution by rotation-invariant twisted photons. *Phys Rev Lett* 113(6):060503.
26. Krenn M, et al. (2014) Communication with spatially modulated light through turbulent air across Vienna. *New J Phys* 16(11):113028.
27. Lavery MP, et al. (2015) Study of turbulence induced orbital angular momentum channel crosstalk in a 1.6 km free-space optical link. *CLEO: Science and Innovations* (Optical Society of America, Washington, DC), pp STu1L-4.
28. Berkhout GC, Lavery MP, Courtial J, Beijersbergen MW, Padgett MJ (2010) Efficient sorting of orbital angular momentum states of light. *Phys Rev Lett* 105(15):153601.
29. Fickler R, Krenn M, Lapkiewicz R, Ramelow S, Zeilinger A (2013) Real-time imaging of quantum entanglement. *Sci Rep* 3:1914.
30. Kim T, Fiorentino M, Wong FN (2006) Phase-stable source of polarization-entangled photons using a polarization Sagnac interferometer. *Phys Rev A* 73(1):012316.
31. Fedrizzi A, Herbst T, Poppe A, Jennewein T, Zeilinger A (2007) A wavelength-tunable fiber-coupled source of narrowband entangled photons. *Opt Express* 15(23):15377–15386.
32. Ho C, Lamas-Linares A, Kurtsiefer C (2009) Clock synchronization by remote detection of correlated photon pairs. *New J Phys* 11(4):045011.
33. Gühne O, Tóth G (2009) Entanglement detection. *Phys Rep* 474(1):1–75.
34. Curtis JE, Grier DG (2003) Structure of optical vortices. *Phys Rev Lett* 90(13):133901.
35. Padgett MJ, Miatto FM, Lavery MP, Zeilinger A, Boyd RW (2015) Divergence of an orbital-angular-momentum-carrying beam upon propagation. *New J Phys* 17(2):023011.
36. Ren Y, Xie G, Huang H, Ahmed N, Yan Y, Li L, Willner AE (2014) Adaptive-optics-based simultaneous pre-and post-turbulence compensation of multiple orbital-angular-momentum beams in a bidirectional free-space optical link. *Optica* 1(6):376-382 (2014).
37. Xie G, et al. (2015) Phase correction for a distorted orbital angular momentum beam using a Zernike polynomials-based stochastic-parallel-gradient-descent algorithm. *Opt Lett* 40(7):1197–1200.
38. Klöckl C, Huber M (2015) Characterizing multipartite entanglement without shared reference frames. *Phys Rev A* 91(4):042339.
39. Gröblacher S, Jennewein T, Vaziri A, Weihs G, Zeilinger A (2006) Experimental quantum cryptography with qutrits. *New J Phys* 8(5):75.
40. Leach J, Bolduc E, Gauthier DJ, Boyd RW (2012) Secure information capacity of photons entangled in many dimensions. *Phys Rev A* 85(6):060304.
41. Mafu M, Dudley A, Goyal S, Giovannini D, McLaren M, Padgett MJ, Forbes A (2013) Higher-dimensional orbital-angular-momentum-based quantum key distribution with mutually unbiased bases. *Phys Rev A* 88(3):032305.
42. Huber M, Pawłowski M (2013) Weak randomness in device-independent quantum key distribution and the advantage of using high-dimensional entanglement. *Phys Rev A* 88(3):032309.
43. Tamburini F, Thidé B, Molina-Terriza G, Anzolin G (2011) Twisting of light around rotating black holes. *Nat Phys* 7(3):195–197.

PHYSICS